Breast Cancer (2011) 18:18–23
DOI 10.1007/s12282-010-0215-8

Histopathological effect of radiofrequency ablation therapy for primary breast cancer, with special reference to changes in cancer cells and stromal structure and a comparison with enzyme histochemistry

Kunihiko Seki · Hitoshi Tsuda · Eriko Iwamoto · Takayuki Kinoshita

Received: 7 April 2010 / Accepted: 7 June 2010 / Published online: 4 August 2010

Abstract Radiofrequency ablation (RFA) therapy is expected to be applicable to small breast cancers, but no criteria for its histopathological effect have yet been established. Using samples obtained from 15 patients who had undergone RFA and subsequent mastectomy, we compared the histopathological changes in the ablated area with the results of histochemical staining based on the reduction of nitroblue tetrazolium chloride (NBT) by nicotinamide adenine dinucleotide (NADH) diaphorase in frozen tissue sections, and looked for histological changes indicative of the effect of RFA on breast cancer. Grossly, the ablated area in most of the tumors was rough, gritty, less moist, and surrounded by a red congestive limbic zone. The ablated area showed no staining by the NADH diaphorase reaction, and cancer cells in the area showed marked destruction characterized by an unclear intercellular boundary, elongated eosinophilic cytoplasm, pyknotic "streaming" nuclei, and a poorly defined nuclear and cytoplasmic texture. At the same time, fibrous connective tissue also showed degenerative changes, becoming densely homogeneous with loss of its delicate wavy structure. The area in which RFA appeared to have been histopathologically effective was mostly concordant with the area in which the NADH diaphorase reaction was negative. In the periphery of the ablated area, however, cellular changes caused by RFA were less marked, although the NADH diaphorase reaction was visualized with NBT. A larger number of cases should be examined in order to establish criteria for the histopathological effect of RFA on breast cancer.

Keywords Breast cancer · Radiofrequency ablation therapy · NADH diaphorase reaction · Histopathological criteria for therapeutic effect

K. Seki (✉)
Clinical Laboratory Division, JR Tokyo General Hospital,
2-1-3 Yoyogi, Shibuya-ku, Tokyo 151-8528, Japan
e-mail: kunihiko-seki@jreast.co.jp

K. Seki · H. Tsuda
Diagnostic Pathology Division,
National Cancer Center Hospital, Tokyo, Japan

E. Iwamoto
Diagnostic Radiology Division,
National Cancer Center Hospital, Tokyo, Japan

T. Kinoshita
Breast Surgery Division,
National Cancer Center Hospital, Tokyo, Japan

Introduction

Radiofrequency ablation (RFA) therapy is expected to be applicable to small breast cancers as an effective and safe curative treatment of choice. However, no criteria for defining its therapeutic effect have yet been established. The majority of previous studies have employed histopathological examination of hematoxylin–eosin (HE)-stained sections and the histochemical technique for visualizing the reduction of nitroblue tetrazolium chloride (NBT) by nicotinamide adenine dinucleotide (NADH) diaphorase in frozen sections.

The NAD+/NADH redox reaction is one of the most important in living biologic systems. NADH diaphorase activity judged from the reduction of NBT to formazan via oxidation of NADH is a reliable marker of cell viability. Assay of NADH diaphorase is performed histochemically using fresh frozen tissue sections. When reduced NADH is

oxidized by NADH diaphorase, free electrons are transferred to NBT, which becomes reduced and converted to the blue, water-insoluble dye formazan (Fig. 1). NADH diaphorase becomes bound to the structural components of the cell, thereby permitting histochemical visualization of its intracellular location by the use of NBT. Only viable cells have active diaphorase, whereas this activity seems to subside immediately after cell death.

On the other hand, several previous reports have described criteria for evaluation of the RFA effect. Jeffrey et al. [1] considered the presence of pyknotic nuclei and increased intensity of eosinophilic staining to be characteristics of tissue cautery due to heating. Earashi et al. [2] applied histopathological criteria for assessment of therapeutic response described in the "General Rules for Clinical and Pathological Recording of Breast Cancer". However, no histopathological criteria for the therapeutic effect of RFA have yet been established.

In the present study, on the basis of a comparison of histopathological changes in the ablated area with the results of histochemical assay with NADH diaphorase, we attempted to characterize the histological changes in breast cancer induced by RFA.

Patients and methods

RFA study protocol

Patient selection and the RFA protocol have been described previously [3]. Histochemical and histopathological examinations were performed on specimens from 15 patients who had undergone RFA for primary breast cancer and subsequent mastectomy between June 2006 and May 2007.

Pathological analysis

After ablation, the surgically resected specimen was cut at the maximum diameter of the ablated breast tumor (Fig. 2). Both the ablated and non-ablated areas of each tumor and adjacent tissue were grossly evaluated, focusing particularly on the features of coagulation, congestion, and elasticity. Slices of tissue, each including apparently ablated and non-ablated areas, were obtained and mounted in optimal cutting temperature (OCT) compound. The tissue was then immediately frozen in liquid nitrogen, and cut into sections 8- to 10-μm thick. One of these sections was immediately stained with HE, and the others were stored at −80°C until NADH diaphorase-NBT studies. The remaining surgically resected specimens were fixed in 10% formalin and processed for routine histopathological examination.

Enzyme histochemical analysis

For enzyme histopathological analysis of ablated breast tumors, frozen tissue sections were incubated for 1 h at 37°C in a solution consisting of 0.8 mg/mL reduced β-NADH (Sigma), 0.5 mg/mL nitroblue tetrazolium (Sigma), and 0.05 M Tris-buffered saline (pH 7.4) (Fig. 3). Each slide was fixed in 10% formalin for 30 min and washed in distilled water for 2 min, then glass coverslips were applied with an aqueous medium.

Mapping and evaluation

Ablated cells were confirmed to be non-viable by their negativity for the oxidation–reduction reaction mediated by NADH diaphorase, whereas residual viable cells were stained blue. By referring to serial sections stained with

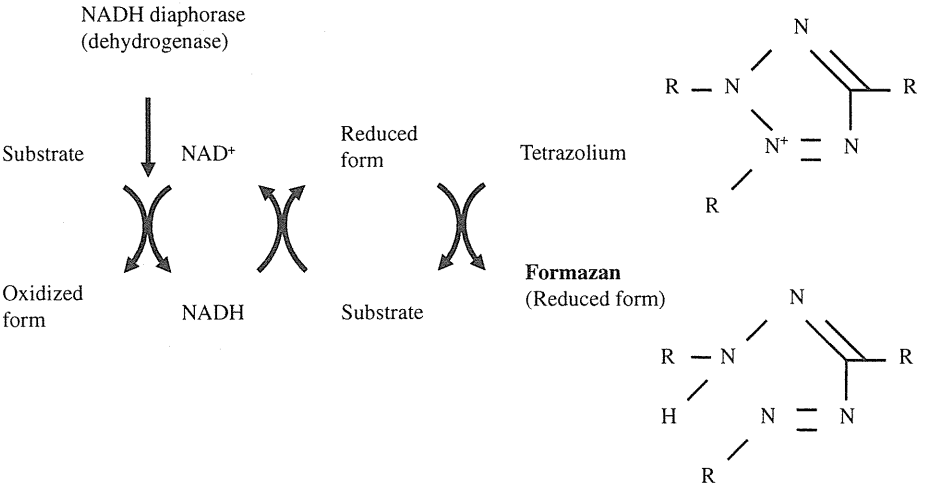

Fig. 1 Nicotinamide adenine dinucleotide (NADH) redox circuit

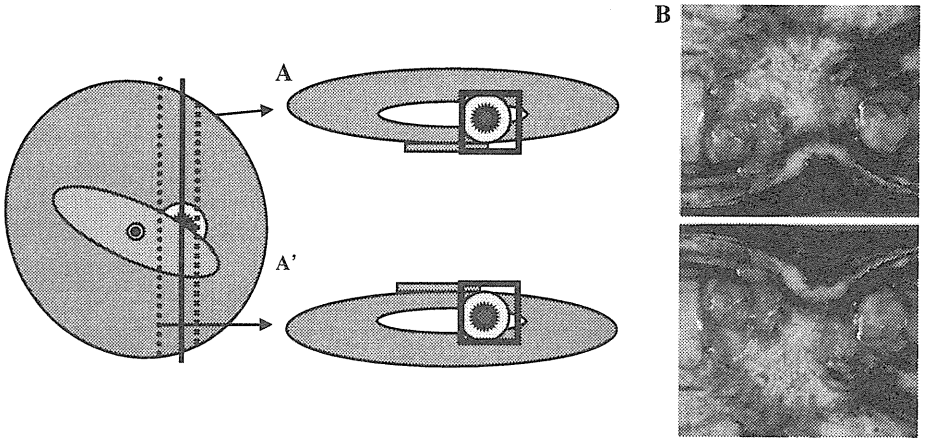

Fig. 2 Schematic representation of tissue specimens used for evaluation of the histopathological effect of radiofrequency ablation (RFA) to primary breast cancer. **a** An ablated tumor cut at the maximum diameter. The tumor in cut section **a** is taken for NADH diaphorase staining. The tumor in cut section **a'**, the mirror image of section **a**, is taken for routine formalin-fixed and paraffin-embedded blocks. **b** Gross features of the ablated tumor. A congestive limbic zone encircles the ablated area containing the tumor

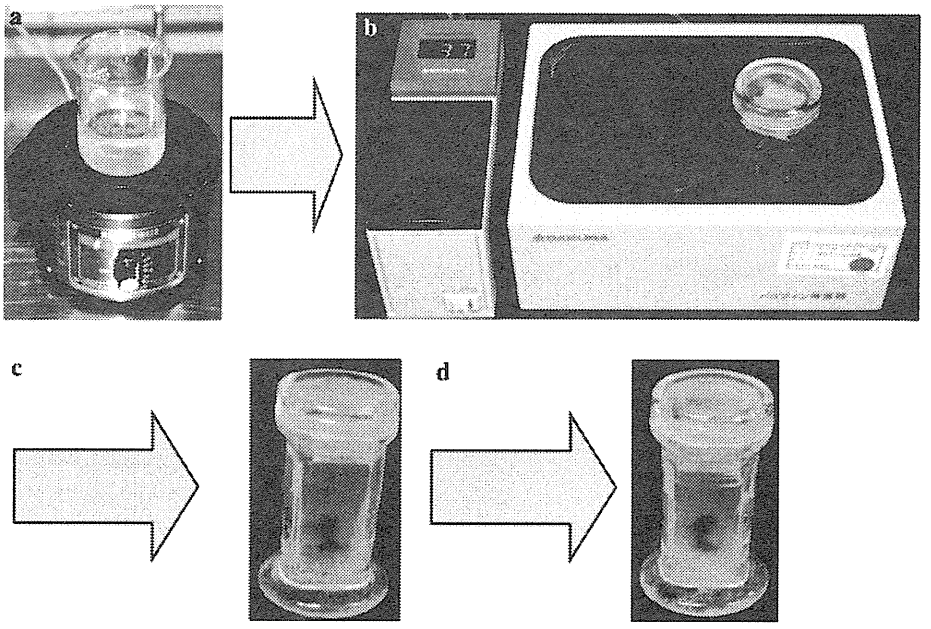

Fig. 3 Preparation of reagents for histochemical assay of nicotinamide adenine dinucleotide (NADH) diaphorase activity. **a** Adjustment of NADH medium. The incubation medium consists of 0.8 mg/mL reduced β-NADH (Sigma), 0.5 mg/mL nitroblue tetrazolium, and 0.05 M Tris-buffered saline (pH 7.4), mixed at 37°C. **b** Fresh frozen tissue sections are incubated in the NADH medium in a water bath at 37°C for 1 h. **c** The tissue sections are washed in distilled water for 2 min. **d** These sections are subsequently fixed in 10% formalin for 30 min

both the NADH diaphorase reaction and HE, we compared the histopathological features of stained and adjacent non-stained areas. Gross and histological features attributable to the thermal effects of RFA were investigated by two pathologists (K.S. and H.T.).

Results

Gross examination

At the cut surface including the tumor, the ablated area felt firmer and more fragile than the surrounding non-ablated area. The cut surface of the ablated area composed of tumor and fibrous stroma was rough, gritty, and less moist, forming a round, flat surface surrounded by swollen fresh, unablated mammary, and fibroadipose tissue (Fig. 4a). In the central zone of the ablated area, the tumor and fibrous connective tissue were grayish-white to tan in color, forming a fissure or small cavity around the needle track (Fig. 4a). Coagulated non-tumor fibroadipose tissue was also firm and had changed to a tan-yellowish color. A red congestive limbic zone surrounded the ablated area (indicated with dots in Fig. 4a). These congestive rings were observed in 14 of 15 cases.

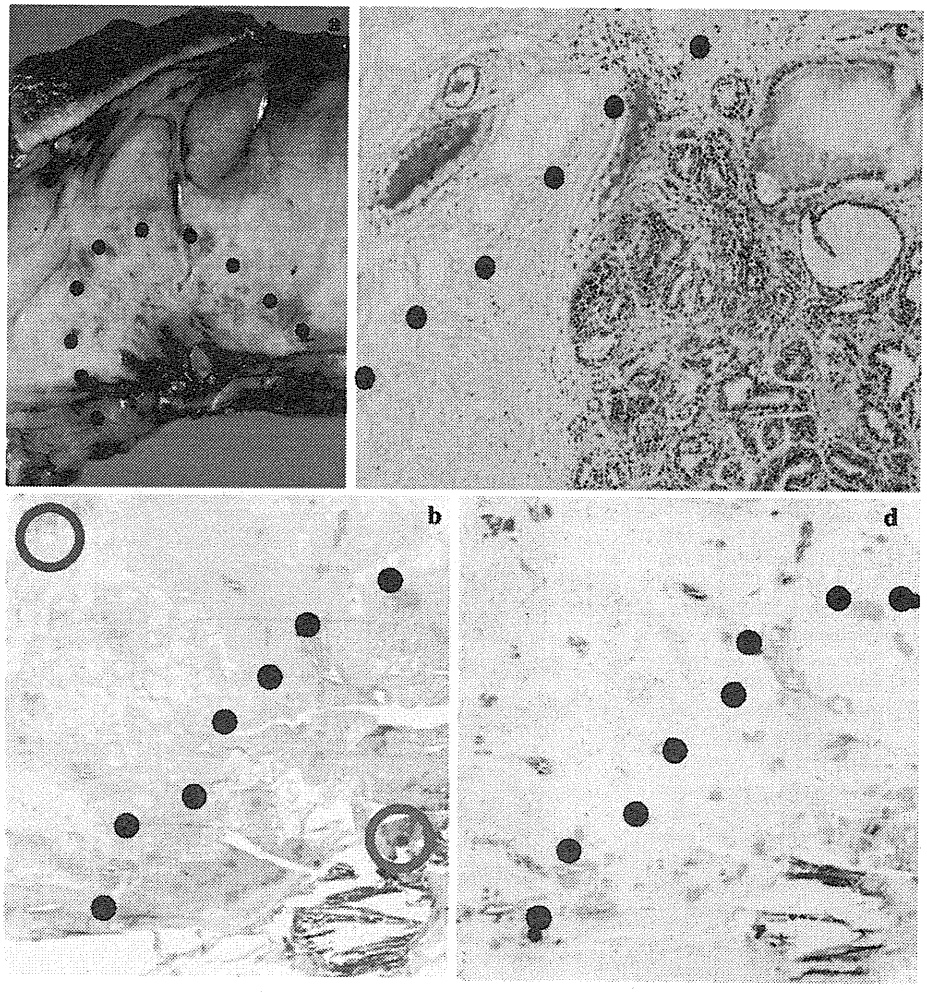

Fig. 4 Macro- and microscopic features of RFA-treated breast cancer and non-cancerous tissue. **a** Gross features of a mastectomized specimen resected immediately after the RFA procedure. The border between the ablated and non-ablated areas is delineated by a congestive limbic zone (indicated by *dots*). **b** The boundary between the ablated area (*right lower* to *dots*) and non-ablated area (*left upper* to *dots*). A low-magnification view of an HE-stained section. The control part of the ablated area (*red circle*) shows highly degenerative changes. **c** A higher-magnification view of the boundary between the ablated (*right lower* to *dots*) and non-ablated (*left upper* to *dots*) areas. In the latter, congestive blood vessels are evident. In the former, mammary tissue and stroma with mild to moderate heating effects are observed (HE). **d** The boundary between the ablated and non-ablated areas in the serial section of image **b**. The section was subjected to the NADH diaphorase reaction to color viable cells blue due to the reduction of NBT. Only the non-ablated area (*left upper* to *dots*) is stained blue

Microscopy examination

The boundary between the ablated and non-ablated area was identifiable histologically, although the effect of cautery showed a gradation from strong in the center to mild or moderate at the periphery (Fig. 4b, c). RFA damage to the epithelial cells and fibrous stroma in the ablated area was histologically visualized as follows in HE-stained sections. Epithelial cells, both cancerous and non-cancerous, were characterized by elongated eosinophilic cytoplasm with pyknotic "streaming" nuclei (Fig. 5b). The intercellular boundary and details of the nuclear and cytoplasmic texture were unclear. Fibrous connective tissue also showed degenerative changes resulting in dense homogeneous and highly eosinophilic features (Fig. 6). The original delicate, wavy structure had entirely disappeared. Fibroblasts in the area also showed thermal degenerative changes identical to those seen in epithelial cells.

At the periphery of the ablated area, epithelial cells showed coarse and plain nuclear chromatin due to the thermal effect (Fig. 5c). The boundary between ablated and non-ablated areas was usually characterized by congestive blood vessels, which were grossly evident as a red limbic zone (Fig. 4a). The effects of heating were sometimes relatively mild to moderate near the limbic zone, because the nuclear and cytoplasmic features characteristic of cell death at the periphery of the ablated area adjacent to the red zone were less marked (Fig. 5c) than those in the central ablated area.

Comparison between NADH diaphorase reaction and histopathological findings

Nicotinamide adenine dinucleotide diaphorase-stained sections showed no reaction in tumor cells at the center of the ablated area, where tumor cells and stroma showed marked heat degeneration. The border between the NADH diaphorase-positive and -negative areas was relatively clear and sharp (Fig. 4d). NADH-positive cells showed the fine structures of intact nuclear chromatin and cytoplasm

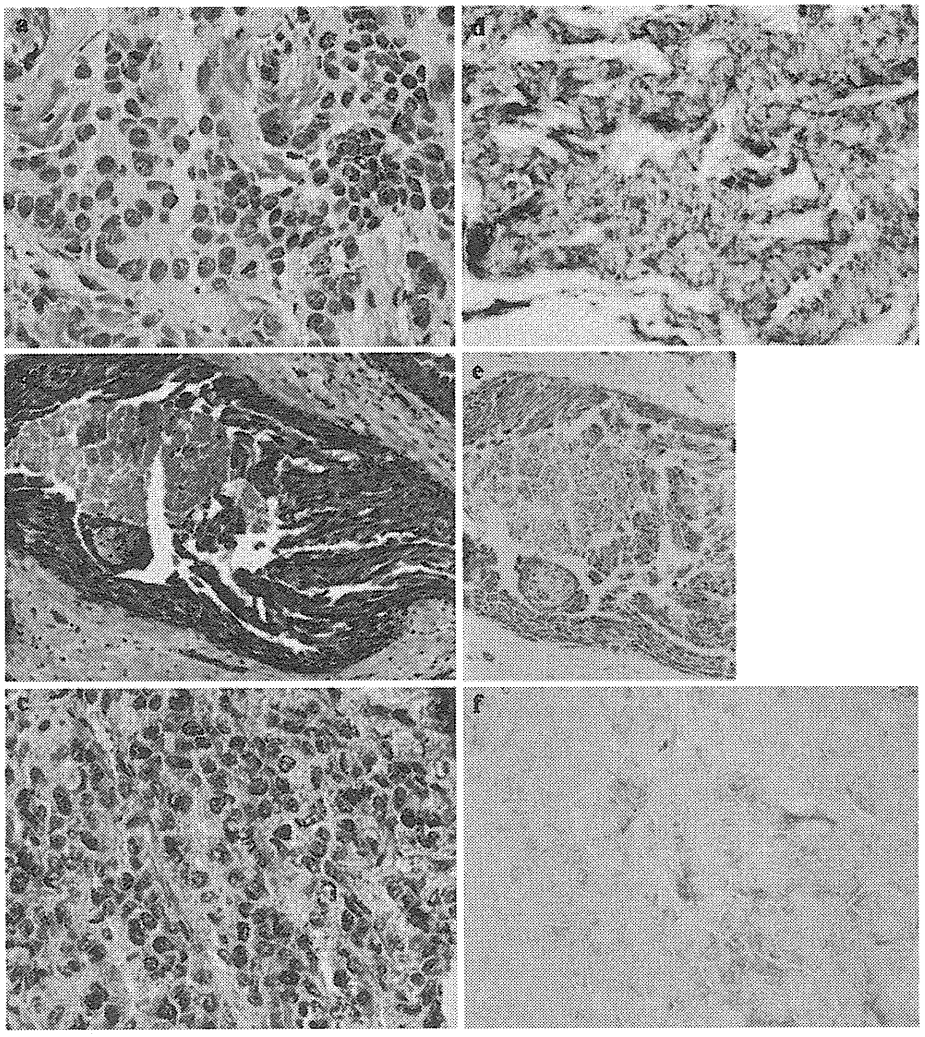

Fig. 5 Comparison of histopathological features of RFA-treated breast cancer tissue with histochemical results of NADH diaphorase staining. **a**, **d** A non-ablated invasive ductal carcinoma (control specimen). **b**, **e** An invasive ductal carcinoma showing a strong effect of RFA cautery. **c**, **f** An invasive ductal carcinoma showing a moderate heating effect of RFA. **a** Fine structure of the nuclei and cytoplasm of tumor cells, and the collagen fibers of the stoma, are preserved. **b** Ablated tumor cells show an elongated cytoplasm with "streaming-like" nuclei. **c** Ablated tumor cells are characterized by pale cytoplasm and rough chromatin in the nuclei with an unclear cellular border. **d** This carcinoma shows a positive NBT reduction reaction, staining the cells blue, indicating histochemical positivity for NADH diaphorase activity. **e** This carcinoma shows a negative reaction for NADH diaphorase, indicating an absence of viable tumor cells. An invasive ductal carcinoma showing a strong cautery effect of RFA. **f** This carcinoma shows a negative reaction for NADH diaphorase, indicating an absence of viable tumor cells

(Fig. 5a, b), surrounded by a fine, delicate fibrous stroma. In each tumor, the NADH-negative area was approximately equivalent to the area circumscribed by the congestive limbic zone. Neither the central area showing strong effects of cautery, nor the peripheral part of the ablated area showing less marked effects showed the NADH diaphorase reaction (Fig. 5d, f).

Discussion

We have described the macro- and microscopic findings characteristic of the cautery or heating effect of RFA, based on examination of specimens resected immediately after the procedure. The histopathological features of cellular damage described by some authors have included an unclear intercellular boundary, elongated eosinophilic cytoplasm, pyknotic "streaming" nuclei, and poorly defined nuclear and cytoplasmic texture [1, 4]. In addition, we found that the RFA procedure caused fibrous connective tissue to lose its delicate wavy structure and to degenerate to dense eosinophilic tissue with a loss of fine structure.

The area in which RFA was histologically effective was mostly concordant with the area of NADH diaphorase negativity, especially in the central part of the ablated area. At the periphery, however, cellular change caused by RFA was less marked, and the NADH diaphorase reaction visualized by NBT was usually negative. Fornage et al. described the histopathological changes observed in RFA-treated breast tissues in a study of 21 patients. The changes were similar to those observed in the present study, and were concordant with the results of NADH diaphorase staining [4]. However, a large number of cases should be studied in order to establish criteria for the histopathological effect of RFA. Although the histochemical assay for NADH diaphorase activity is reliable, it cannot always be performed in routine practice. It will therefore be necessary

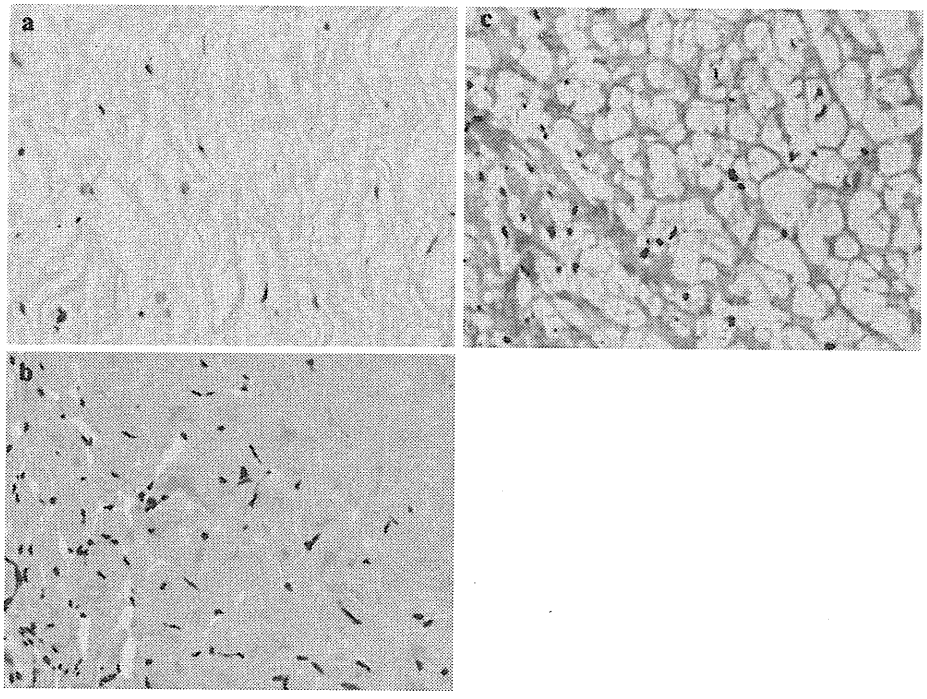

Fig. 6 **a** Non-ablated stromal tissue in the breast demonstrates the fine wavy structure of collagen fibers (control specimen). **b**, **c** A highly ablated stroma showing eosinophilic and amorphous features without a fine wavy texture. Nuclei of fibroblasts are also pyknotic

to standardize criteria for the effects of RFA that are applicable to formalin-fixed and paraffin-embedded tissue sections.

Acknowledgments This work was supported in part by a grant-in-aid for scientific research from the Ministry of Heath, Labor and Welfare, Japan.

References

1. Jeffrey SS, Birdwell RL, Ikeda DM. Radiofrequency ablation of breast cancer: first report of an emerging technology. Arch Surg. 1999;134:1064–8.
2. Earashi M, Noguchi M, Motoyoshi A, Fujii H. Radiofrequency ablation therapy for small breast cancer followed by immediate surgical resection or delayed mammotome excision. Breast Cancer. 2007;14:39–47.
3. Kinoshita T, Iwamoto E, Tsuda H, Seki K (2010) Radiofrequency ablation as local therapy for early breast carcinomas. Breast Cancer. doi:10.1007/s12282-009-0186-9
4. Fornage BD, Sneige N, Ross MI, Mirza AN, Kuere HM, Edeiken BS, et al. Small (≤2-cm) breast cancer treated with US-guided radiofrequency ablation: feasibility study. Radiology. 2004; 231:215–24.

Breast Cancer (2011) 18:24–32
DOI 10.1007/s12282-010-0222-9

A histopathological study for evaluation of therapeutic effects of radiofrequency ablation in patients with breast cancer

Hitoshi Tsuda · Kunihiko Seki · Takahiro Hasebe · Yuko Sasajima · Tatsuhiro Shibata · Eriko Iwamoto · Takayuki Kinoshita

Received: 20 July 2010 / Accepted: 24 August 2010 / Published online: 23 September 2010

Abstract
Purpose To reveal the rate of complete therapeutic effect of radiofrequency ablation (RFA) and its correlation with tumor size by the histopathological examination of surgically resected early breast cancers.
Methods For 28 patients who received RFA and subsequent surgical therapies for early breast cancer treatment, the effect of RFA was evaluated by both histopathological examination and nicotinamide adenine dinucleotide (NADH)-diaphorase staining of resected tumor specimens according to the criteria described by Seki et al. (this issue). The correlation of 100% RFA effect with tumor parameters including tumor size and the presence of extensive intraductal component (EIC) was examined.
Results The mean size and invasive size of the primary tumors were 2.21 cm (ranging from 0.6 to 5.0 cm) and 1.44 cm (ranging from 0 to 5.0 cm), respectively. By examining hematoxylin-eosin (HE) sections, the effectiveness of RFA was found to be 100% in 16 tumors (57%). However, the effectiveness of RFA was found to be 100% in 22 cases (79%) examined by NADH-diaphorase staining of frozen sections containing part of tumorous and nontumorous tissues. The accuracy of diagnosis of complete RFA effect using NADH-diaphorase staining with reference to HE was 79% (22 of 28) with 100% (16 of 16) sensitivity and 50% (6 of 12) specificity. The rate of 100% RFA effect by HE examination was higher in EIC(−) tumors (13 of 17, 76%) than in EIC(+) tumors (1 of 9, 11%) ($P = 0.0022$), and was higher in tumors of ≤1.5 cm (10 of 11, 91%) than in tumors of >1.5 cm (6 of 17, 35%; $P = 0.0034$). All five tumors of ≤1.0 cm showed 100% RFA effect, but 3 (27%) of 11 tumors of >1.0 and ≤2.0 cm and 9 (75%) of 12 tumors of >2.0 cm showed suboptimal RFA effect by HE.
Conclusions Tumor size of ≤1.5 cm, strictly ≤1.0 cm, could be an indication for RFA if a complete histological therapeutic effect is mandatory.

Keywords Radiofrequency ablation · Breast cancer · Therapeutic effect · NADH diaphorase

H. Tsuda (✉) · T. Hasebe · Y. Sasajima · T. Shibata
Pathology and Clinical Laboratory Division, National Cancer Center Hospital, 5-1-1 Tsukiji, Chuo-ku, Tokyo 104-0045, Japan
e-mail: hstsuda@ncc.go.jp

K. Seki
Clinical Laboratory Division, JR Tokyo General Hospital, 2-1-3 Yoyogi, Shibuya-ku, Tokyo 151-8528, Japan

T. Hasebe
Pathology Consultation Service, Clinical Trials and Practice Support Division, Center for Cancer Control and Information Services, National Cancer Center, 5-1-1 Tsukiji, Chuo-ku, Tokyo 104-0045, Japan

T. Shibata
Cancer Genomics Project, Center for Medical Genomics, National Cancer Center Research Institute, 5-1-1 Tsukiji, Chuo-ku, Tokyo 104-0045, Japan

E. Iwamoto · T. Kinoshita
Surgical Oncology Division, National Cancer Center Hospital, 5-1-1 Tsukiji, Chuo-ku, Tokyo 104-0045, Japan

Introduction

Histopathological evaluation of radiotherapeutic effects in patients' cancerous tissues, including esophageal or cervical cancers, was established in Japan in the 1960s [1]. This system evaluates the percentage of area with markedly altered, presumably nonviable cancer cells, and the area

Table 1 Pathological findings and therapeutic effects in 28 tumors subjected to radiofrequency ablation (RFA)

No./age	Permanent section												Frozen section	
	Histology	Grade	pN	ER	PR	HER2	Tumor size (cm)	Invasive size (cm)	Daughter nodule	EIC	Area with RFA effect (cm)	RFA effect (HE) (%)	Tumor size in sample	NADH effect (%)
1/52/L	muc	1	0	2	0	1	2.4	2.4	–	–	6.6	100	1.6	100
2/69/R	Pred DCIS	1	0	3	1	1	2.2	0.08	–	NA	3.2	100	0.8	100
3/79/R	IDC(pap)	2	0	3	3	0	2.1	2.1	–	–	6	100	1.2	100
4/67/L	IDC(sol)	3	0	0	0	0	2	1.7	–	–	4.2	100	1.7	100
5/64/R	IDC(sol)	3	0	0	0	1	1.7	1	–	–	5.5	100	1.3	100
6/68/L	IDC(sci)	3	0	0	0	0	1.6	1.6	–	–	3.5	100	1.3	100
7/54/L	IDC(pap)	1	0	3	1	1	1.5	0.8	–	+	5.8	100	0.3	100
8/62/L	IDC(sol)	2	0	3	3	0	1.5	1.5	+	–	2.7	100	1.3	100
9/53/R	IDC(sci)	2	0	3	3	0	1.3	1.3	–	–	2.8	100	1.1	100
10/36/R	IDC(pap)	1	0	2	0	0	1.2	1.2	–	–	3.4	100	0.9	100
11/82/R	IDC(sci)	1	0	2	3	1	1.1	1.6	–	–	4	100	1	100
12/47/L	IDC(pap)	1	0	3	3	1	1	0.7	–	–	1.9	100	1	100
13/66/R	DCIS	NA	0	0	0	1	0.9	0	–	NA	4	100	0.8	100
14/67/L	IDC(sci)	2	1	3	2	1	0.8	0.8	–	–	3.7	100	0.9	100
15/42/R	IDC(pap)	1	1	2	2	0	0.6	0.5	–	–	3	100	0.7	100
16/38/L	IDC(pap)	1	0	1	0	1	0.5	0.2	–	–	2.4	100	0.5	100
17/52/R	IDC(sci)	1	3	3	3	0	5	5	–	–	5	90–95	2	90–95
18/45/L	IDC(pap)	1	3	1	3	1	4.7	1.1	+	+	3.9	30	0.5	100
19/57/L	IDC(sol)	1	0	3	2	0	4.7	2.1	–	+	1.7	40	0.7	90
20/78/R	IDC(pap)	1	1	3	0	0	4.2	1.2	–	+	4.7	95	1.2	100
21/48/R	IDC(sci)	2	0	1	3	0	4	2.4	–	+	4	60	1.3	90
22/59/L	IDC(sol)	3	0	0	0	3	3.5	2.6	–	+	3.9	40–50	1.5	40–50
23/62/R	IDC(pap)	1	0	3	3	1	3.2	1.1	–	+	2.6	60–70	1.6	80
24/73/L	IDC(sci)	1	0	3	1	1	2.5	2.5	–	–	3.3	90	1.4	100
25/60/L	IDC(sol)	1	0	3	3	0	2.5	1	–	+	2.5	95	1	100
26/43/L	IDC(sci)	1	0	3	3	1	2	0.8	–	–	2.5	95	0.4	100
27/63/L	IDC(pap)	1	0	3	3	1	1.8	1.5	–	+	1.7	80	1.5	0
28/69/L	muc	1	0	3	0	0	1.5	1.5	–	–	5.5	95	1.3	100

Tumor size includes both invasive and intraductal components

DCIS ductal carcinoma in situ, *EIC* extensive intraductal component, *ER* estrogen receptor, *HE* hematoxylin-eosin, *HER2* human epidermal growth factor receptor 2, *IDC* invasive ductal carcinoma, *L* left, *muc* mucinous carcinoma, *NA* not applicable, *NADH* nicotinamide adenine dinucleotide-diaphorase, *pap* papillotubular carcinoma, *PR* progesterone receptor, *Pred DCIS* predominantly DCIS, *R* right, *sci* scirrhous carcinoma, *sol* solid-tubular carcinoma

from where cancer cells had disappeared [1]. The application of this classification was extended to evaluation of chemotherapeutic effects in 1985 and adopted in the 11th edition of the General Rules for the Gastric Cancer Study [2]. However, it was very difficult to determine correctly whether the altered cancer cells were viable.

In the NSABP-B-18 trial of neoadjuvant chemotherapy for patients with breast cancer, a histopathological evaluation system for chemotherapeutic effects was adopted solely on the basis of the presence or absence of invasive cancer cells, regardless of the degree of cellular degeneration or viability [3]. Thereafter, in different histopathological criteria used for evaluating therapeutic effects in breast cancers by using neoadjuvant chemotherapy, the evaluation was done usually on the basis of the presence of residual tumor cells, regardless of the extent of alteration of residual cancer cells [4, 5]. Because the sensitivity of cancer cells against chemo- or radiotherapy differs among cases, and the extent of therapeutic effects was shown to be correlated with patients' prognosis, accurate histopathological assessment of therapeutic effects has come to be required by clinical oncologists to pathologists as a routine activity. Because sometimes the pathological complete response (pCR) is set as the primary end point of clinical studies of neoadjuvant therapies to breast cancers [6–8], evaluation is frequently conducted in the form of a central pathological review [7, 8].

Recently, radiofrequency ablation (RFA) has been introduced in the field of breast cancer therapy [9, 10]. Because the effect of RFA is evaluated by cautery effect, which is almost common among tumors if the conditions of operation were uniform, establishment of common criteria for assessing therapeutic effects would be very useful to pathologists. In general, evaluation is performed by a combination of hematoxylin and eosin (HE) staining and nicotinamide adenine dinucleotide (NADH)-diaphorase

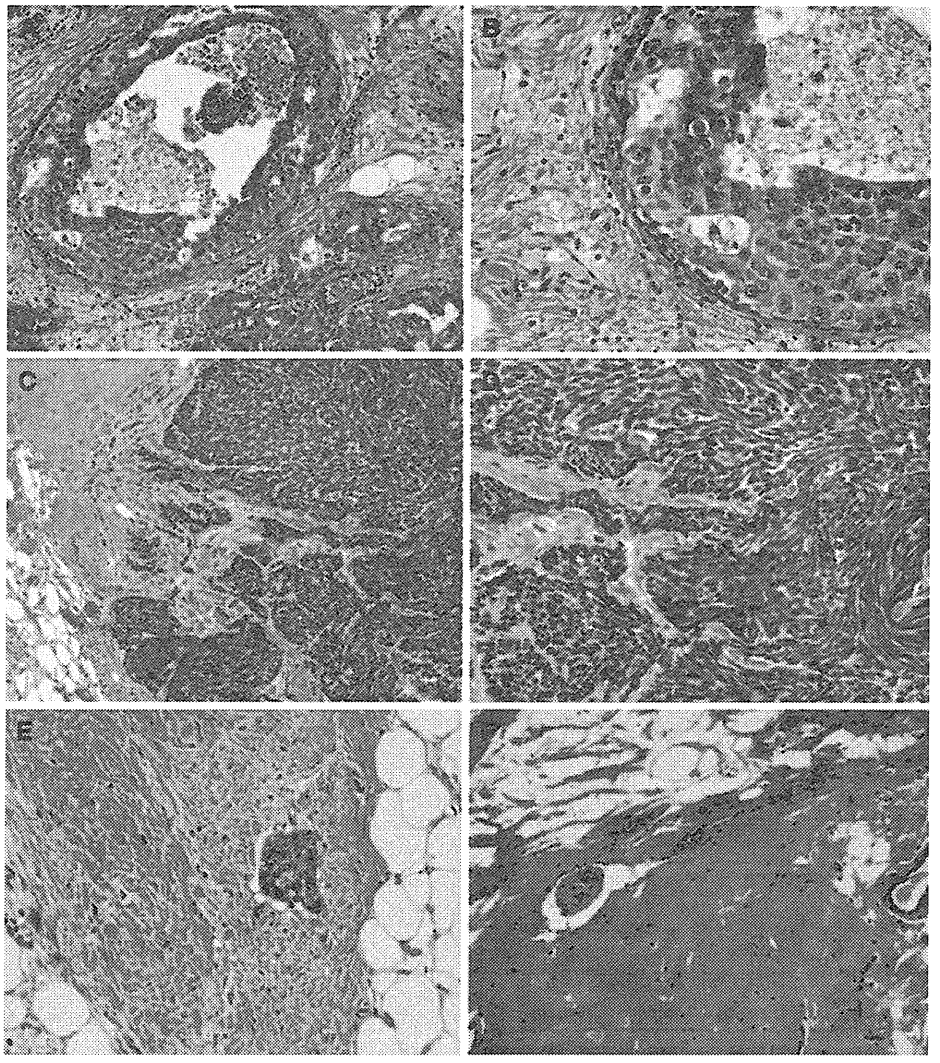

Fig. 1 Alterations in breast cancer and noncancerous tissues by radiofrequency ablation (RFA). **a**, **b** In situ component of a ductal carcinoma without RFA effect. Cancer cells and stromal lymphocytes are viable without degenerative changes, and the morphology of stromal collagen fiber is well preserved. **c**, **d** Invasive carcinoma component with RFA effect. Cancer cells and stromal cells show pyknotic "streaming" nuclei, unclear intercellular boundaries, and unclear nuclear and cytoplasmic morphological details. In stroma, collagen fibers show degenerative changes. **e** Breast stromal tissue without RFA effect. The morphology of stromal collagen fibers is well preserved. A cancer cell nest is also seen. **f** Noncancerous stromal tissue with RFA effect. In stroma, collagen fibers show degenerative changes resulting in dense homogeneous and highly eosinophilic features. ×100 in **a**, **c**, **e**, and **f**, and ×200 in **b** and **d**. ×100 in **a** and **c**, and ×200 in **b** and **d**

staining (reviewed in ref. [11]). Although several studies have shown that evaluation of the therapeutic effects by using NADH-diaphorase staining is useful, evaluation of therapeutic effects by RFA would become more reproducible and accurate if evaluations are effectively done using HE-stained sections of formalin-fixed, paraffin-embedded tissues. Seki et al. [11] have described criteria for histopathological evaluation of RFA effects in breast cancers.

In the present study, RFA effects assessed by HE staining were compared with those assessed by NADH-diaphorase staining of surgically resected breast-cancer tissues, which were obtained immediately after RFA application in a pilot study to examine the safety and efficacy of RFA [9, 11]. In addition, we examined the parameters that caused suboptimal histopathological therapeutic effects in the tumor treated by RFA.

Patients and methods

RFA study protocol

This study was approved by the Institutional Review Board for ethical issues in the National Cancer Center, Japan. All the patients provided written informed consent. The criteria for patient selection and the RFA protocol have been previously described [9]. Under ultrasound guidance, RFA was performed using the 17-gauge Valleylab RF Ablation System with Cool-tip Technology (Covidien, Energy-Based Devices, Interventional Oncology, Boulder, CO) [9]. Histochemical and histopathological examinations of specimens from 28 patients who underwent RFA for primary breast cancer and subsequent partial breast resection or mastectomy between June 2008 and May 2009 were performed. For RFA, radiofrequency energy was sufficient in 19, but the increase of the energy during the procedure was suboptimal in 2 cases (cases 23 and 27 in Table 1).

After ablation, the surgically resected specimens were subjected to sampling of tumor and control tissues for NADH-diaphorase staining. From the representative cut surface of the ablated tumor, at least two thinly sliced sections 2–3 cm in size were removed and prepared as frozen sections: one section contained an apparently ablated area and a representative cut surface of the main tumor, and the other contained non-tumor areas without RFA effect. These tissues were mounted in Cryo Mount I (Muto Pure Chemicals, Tokyo, Japan), immediately frozen on dry ice, and cut into 8- to 10-μm-thick sections. One of these sections was stained with HE, and the others were stored at −80°C until NADH-diaphorase staining.

Enzyme histopathological analysis of the ablated breast tumors was performed according to a method described by Seki et al. [11] and Imoto et al. [12]. The ablated areas were confirmed to contain dead cells, which were negative for the oxidation-reduction reaction mediated by NADH-diaphorase, whereas residual live cells stained blue. We compared the histopathological features of the stained with the unstained adjacent areas by using serial sections stained with both the NADH-diaphorase reaction and HE. The histopathological features attributable to the thermal effects of RFA were investigated by two pathologists.

The remaining surgically resected specimens were fixed in 10% formalin and processed for routine histopathological examination. For partially resected breast specimens, a total of ~20–30 tissue blocks were all sectioned. For total mastectomy specimens, more than 15 tissue blocks were made, all including entire tumor areas. If necessary, additional cutting was performed after initial histological examinations. The ablated areas and ablated tumorous areas were mapped on cut sections, and on the basis of this map, the percentage areas containing tumorous tissue was estimated by at least 2 pathologists.

For both frozen sections and formalin-fixed, paraffin-embedded sections stained with HE, RFA damage to the epithelial cells and fibrous stroma was histologically evaluated according to the criteria described by Seki et al. [11]. In brief, the area with RFA effect in HE-stained sections was histologically visualized as follows (Fig. 1).

Table 2 Summary of the profiles of 28 primary breast carcinomas subjected to radiofrequency ablation (RFA) and subsequent partial resection of the breast or mastectomy

Mean tumor size (total)	2.21 cm (0.6–5.0) (1.31 SD)
Mean tumor size (invasion)	1.44 cm (0–5.0) (1.00 SD)
Mean size of degenerated area by RFA	3.71 cm (1.7–6.0) (1.33 SD)
Incidence of 100% RFA effect by HE staining in primary tumor	16/28 (57%)
Incidence of 100% RFA effect by NADH-diaphorase staining in primary tumors	22/28 (79%)
Concordance between RFA effect by HE and RFA effect NADH-diaphorase staining	22/28 (79%)

Tumor size (total) includes both invasive and intraductal components

HE hematoxylin and eosin, *NADH* nicotinamide adenine dinucleotide, *SD* standard deviation

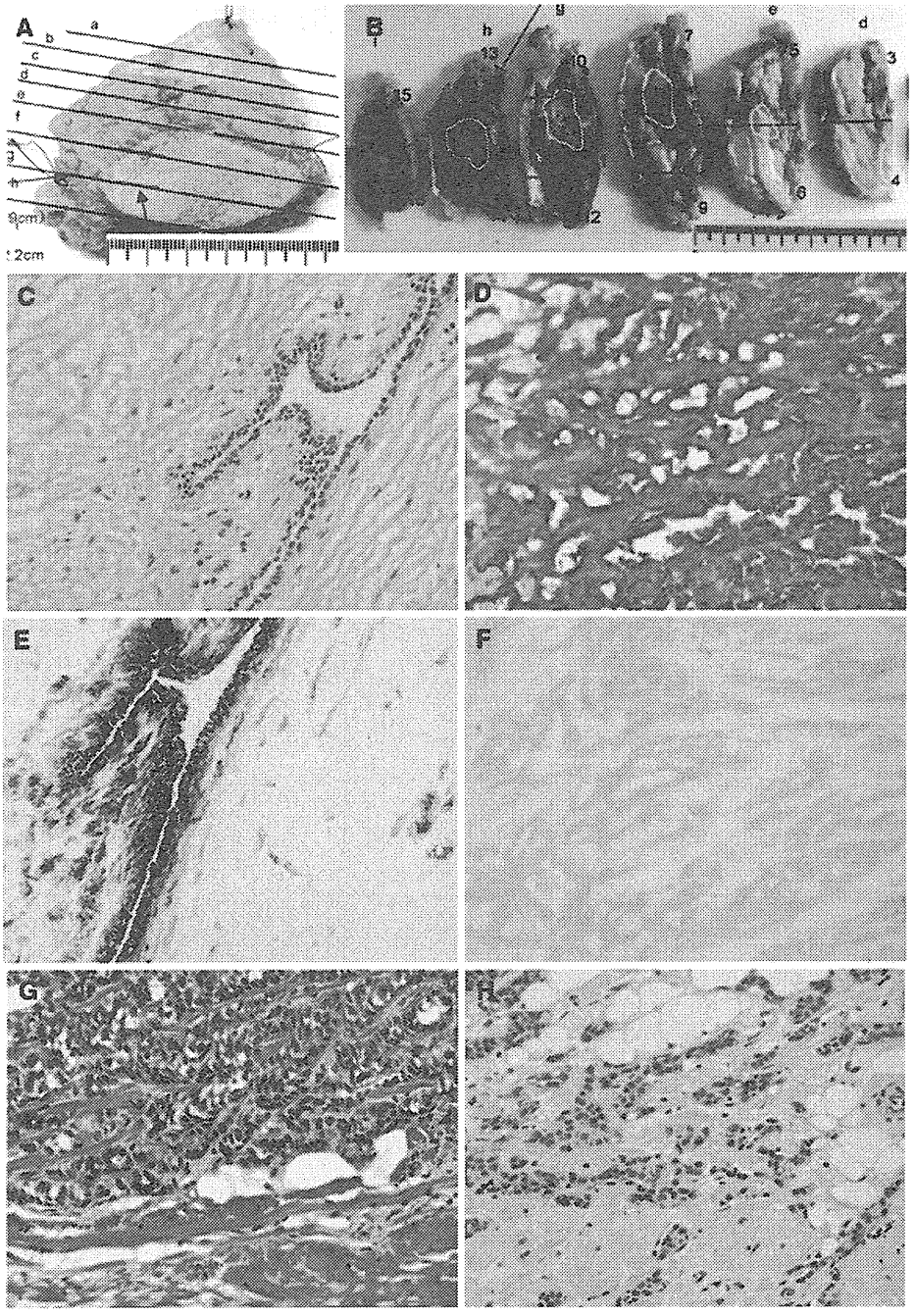

Fig. 2 A case with 100% effective RFA in the main tumor but no effect in the daughter lesion assessed by hematoxylin and eosin (HE) staining. **a**, **b** Surgically resected specimens. *Areas* in *red* represent invasive carcinoma components. Ablated areas are circumscribed in *green*. An *arrow* indicates the daughter lesion. **c**, **d** Frozen sections of the resected tissue specimens stained with HE. **c** Viable non-tumor area with no histopathological RFA effect. No degradation changes are seen in epithelial cells and stromal structures. **d** Tumor area with a strong histopathological RFA effect. Tumor tissues had lost intercellular boundaries and nuclear or cytoplasmic morphological details. Fibrous connective tissue is also highly degenerated into a densely homogeneous and highly eosinophilic structure. **e**, **f** Nicotinamide adenine dinucleotide (NADH)-diaphorase reaction of serial sections of **c** and **d**. **e** NADH diaphorase in a histopathologically viable area. **f** NADH diaphorase in an area with highly degenerated histopathological features. **g**, **h** Permanent sections stained with HE. **g** Histopathologically highly degenerated tumor area (*upper*) and stromal area (*lower*). **h** Histopathological features of the daughter lesions in which no RFA effect is seen. ×100

Epithelial cells, both cancerous and noncancerous, were characterized by elongated eosinophilic cytoplasm with pyknotic "streaming" nuclei. The intercellular boundaries and details of the nuclear and cytoplasmic morphology were unclear (Fig. 1a–d). Fibrous connective tissue also showed degenerative changes with dense homogeneous and highly eosinophilic features. The original delicate, wavy appearance entirely disappeared. Fibroblasts in the area also showed thermal degenerative changes identical to those seen in epithelial cells (Fig. 1e, f).

Statistical analysis

Statistical difference was analyzed by Fisher's exact test.

Results

The findings of pathological examination of the 28 tumors subjected to RFA are presented in Tables 1 and 2. In the Tables, tumor size or tumor size (total) means to the largest

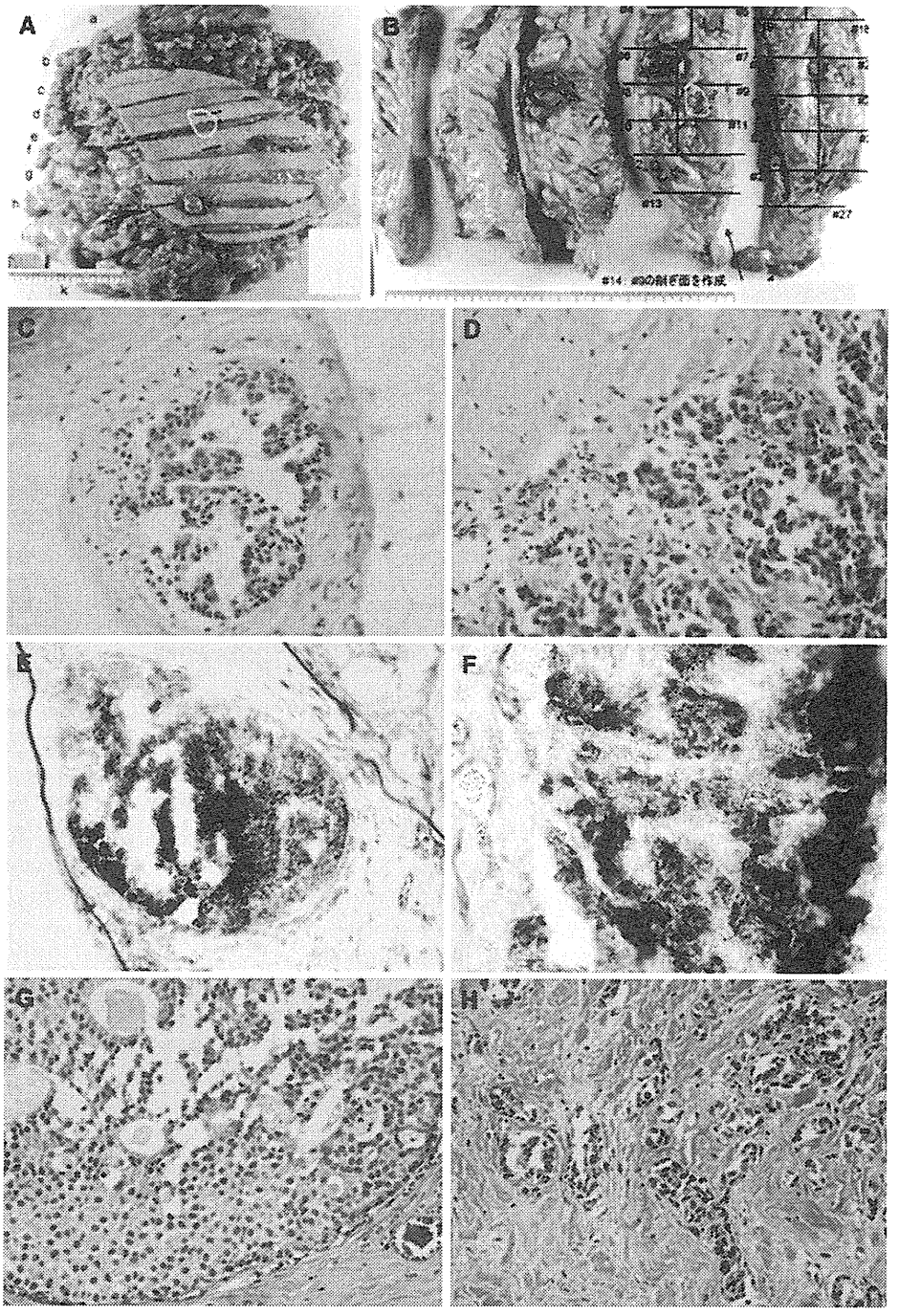

Fig. 3 A case in which histological evaluation of RFA effect was 80% by HE, but the effect was absent by NADH-diaphorase staining. **a**, **b** Surgically resected specimens. *Areas* in *red* and *blue* represent invasive carcinoma and ductal carcinoma in situ (DCIS), respectively. Ablated areas are represented in *yellow*. **c**, **d** Frozen sections of the tumor tissue stained with HE. **c** A viable area without histopathological RFA effect. No degradation changes are seen in either tumor or stromal tissues. **d** An area with histopathological RFA effect. The cells of the tumor tissue show elongated eosinophilic cytoplasm with pyknotic nuclei. **e**, **f** NADH-diaphorase reaction. The results of NADH-diaphorase staining were positive in both histologically viable and nonviable tissue areas in series with **c** and **d**. **g**, **h** Formalin-fixed, paraffin-embedded sections stained with HE. **g** Histopathologically viable DCIS area. **h** Histopathologically highly degenerated invasive carcinoma area. Findings are the same as those in **d**; ×100 in **c** and **e**; ×200 in **d**, **f**, **g** and **h**

diameter of the tumor, including invasive carcinoma and intraductal carcinoma components and including both ablated and non-ablated tumor area. Histological grades of the tumors were 1, 2, and 3 in 18, 5, and 4, respectively. Grading of one tumor could not be determined because of marked degenerative changes. The mean tumor size, including both invasive and noninvasive components, was 2.21 cm, ranging from 0.6 to 5.0 cm. The mean size of invasive components was 1.44 cm, ranging from 0 [ductal carcinoma in situ (DCIS)] to 5.0 cm. An extensive intraductal component (EIC) was positive in 9 tumors, but negative in 17 tumors. One case of DCIS and one case of invasive ductal carcinoma with a predominantly DCIS component were included in the study.

The mean size of the degenerated areas by RFA, including both tumorous and the surrounding nontumorous

Table 3 Factors correlated with 100% radiofrequency ablation (RFA) effect by hematoxylin eosin (HE) findings

Factor	Number of tumors (%) RFA effect by HE			P
	Total	100% Effect	<100% Effect	
Extensive intraductal component (EIC)				
EIC(+)	9	1 (11)	8 (89)	0.0022
EIC(−)	17	13 (76)	4 (24)	
DCIS	2	2 (100)	0 (0)	
Tumor size (total, cutoff 1.5 cm)[a]				
≤1.5 cm	11	10 (91)	1 (9)	0.0034
>1.5 cm	17	6 (35)	11 (65)	
Tumor size (total, cutoff 1.0 cm and 2.0 cm)				
≤1.0 cm	5	5 (100)	0 (0)	0.0037
>1.0 cm, ≤2.0 cm	11	8 (73)	3 (27)	
>2.0 cm	12	3 (25)	9 (75)	

Tumor size (total) includes both invasive and intraductal components

DCIS ductal carcinoma in situ, *EIC* extensive intraductal component

[a] One tumor of ≤1.5 cm but <100% RFA effect was 1.5 cm in diameter, and the effect was 95% by HE and 100% by NADH-diaphorase staining

tissues, was 3.71 cm, ranging from 1.7 to 6.0 cm. Incidence of a 100% effective RFA by HE was 57% (16 of 28) in primary tumors. Of these 16 cases, 1 had a daughter nodule, and because RFA was performed only for the main tumor, the therapeutic effect was 100% for the main tumor, but the effect was absent for the daughter nodule (Fig. 2). By HE, in tumors with incomplete RFA effect, the area of RFA effect was evaluated to be ≥90% in 6, whereas the area was evaluated to be <90% in 6, including 2 tumors (cases 23 and 27 in Table 1), which were potentially subjected to a suboptimal increase in energy during the RFA procedure.

Nicotinamide adenine dinucleotide-diaphorase staining was positive for all sections containing nonablated areas. In the ablated tissues, tumorous tissue, and surrounding non-tumorous tissue, the size of tumor detected by the NADH-diaphorase staining varied from 0.3 to 2.0 cm (mean 1.10 cm). The incidence of 100% effective RFA detected by NADH-diaphorase staining was 79% (22 of 28) in the primary tumors. The therapeutic effect evaluated by NADH-diaphorase staining was 100% in 22 tumors, <100% but ≥90% in 3 tumors. For the other 3 tumors, the RFA effect evaluated by NADH-diaphorase staining was ≤80%: 2 of these were patients 23 and 27, in whom the radiofrequency energy did not increase optimally. In case 27, histological evaluation of the RFA effect was 80% by HE, but the effect was absent by NADH-diaphorase staining because the results of the latter staining were positive in the entire specimen examined (Fig. 3). Concordance between HE findings and NADH findings of the RFA effect was 79% (22 of 28). The specificity and sensitivity of NADH-diaphorase results (complete or incomplete RFA effect) to HE results (complete or incomplete RFA effect) were 100% (16 of 16) and 50% (6 of 12), respectively.

A 100% effective RFA evaluated by HE staining was correlated with EIC(−) and tumor size (Table 3). A 100% effective RFA was observed in 13 (76%) of the 17 EIC(−) tumors, whereas a 100% effective RFA was observed in only 1 (11%) of the 9 EIC(+) tumors ($P = 0.0022$; Fig. 4). Two cases of DCIS showed 100% RFA effect.

Likewise, a 100% effective RFA evaluated by HE staining was correlated with tumor size, including intraductal component (Table 3): a 100% effective RFA was observed in 10 (91%) of 11 tumors of ≤1.5 cm in diameter, whereas a 100% effective RFA was observed in only 6 (35%) of 17 tumors of >1.5 cm in diameter ($P = 0.0034$). One case of ≤1.5 cm, but <100% effective RFA was 1.5 cm in diameter, and the effect was observed in 95% of the area by HE and 100% of the area by NADH-diaphorase staining.

When tumor size, including intraductal component, was stratified into three categories, 100% effects of RFA were detected in all 5 (100%), 3 (27%) of 11, and 9 (75%) of 12 in tumor groups of tumor size ≤1.0 cm, >1.0 cm but ≤2.0 cm, and >2.0 cm, respectively (Table 3). The rate of a 100% effect of RFA was significantly higher in the patients with a tumor of ≤1.0 cm in size than in those with a tumor of >1.0 cm ($P = 0.0037$).

Discussion

In this study, we evaluated the RFA effect by both HE and NADH-diaphorase staining in 28 primary breast cancers resected from patients immediately after RFA procedures. As studied by Seki et al. [11], therapeutic effects of RFA evaluated by HE were mostly concordant with the loss of cellular viability evaluated by NADH-diaphorase staining. Because the area examined in HE-stained sections was wider (2.21 cm on an average) than the area examined in NADH-diaphorase-stained sections (1.10 cm on an average), the percentage of 100% effective RFA became lower in the former (57%) than in the latter (79%). In 1 case (case 27), there was a discrepancy in the RFA effect between the HE and NADH staining in frozen sections, but examinations of the tumor tissue in formalin-fixed sections stained with HE revealed that HE findings were concordant between frozen sections and the formalin-fixed ones. From these results, only frozen-sectioning examination did not completely and accurately clarify the status of the RFA effect in the entire tumor tissue.

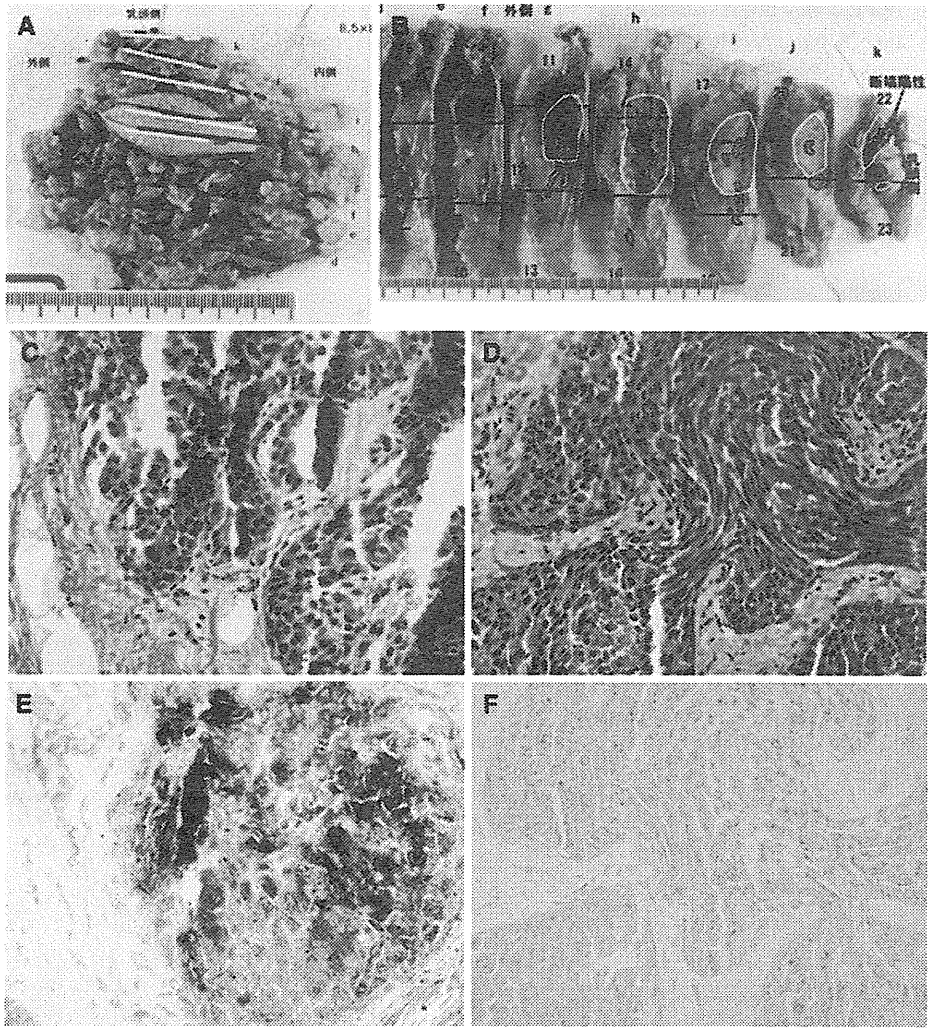

Fig. 4 A case of breast carcinoma, extensive intraductal component (EIC)(+), with 60% effective RFA detected by HE staining of the sections. **a**, **b** Surgically resected specimens. *Areas* in *red* and *blue* represent invasive carcinoma and DCIS, respectively. Ablated areas are represented in *yellow*. **c**, **d** Frozen sections of the tumor tissue stained with HE. **c** Viable area without histopathological RFA effect. No degradative changes are seen in both tumor and stromal tissues. **d** An area with histopathological RFA effect. The cells of the tumor tissue show elongated eosinophilic cytoplasms with pyknotic "streaming" nuclei, unclear intercellular boundaries, and unclear morphological details in the nuclear or cytoplasmic features. Fibrous connective tissue also shows degenerative changes, resulting in dense homogeneous and highly eosinophilic features. **e**, **f** NADH-diaphorase reaction. **e** The results of NADH-diaphorase staining in histopathologically viable areas are positive. **f** NADH diaphorase in the area with histopathological RFA effect shows no reaction. ×200

Nonetheless, if the tumor size was small (≤1.5 cm) and the tumor lacked the EIC component, the proportion of cases with complete RFA effect became very high. In particular, complete RFA effects were observed in all tumors with a diameter of ≤1.0 cm. In these cases, if RFA therapy was conducted with subsequent follow-ups, examination of the therapeutic effect by means of core-needle/mammotome biopsy would be potentially sufficient. In contrast, the ratio of suboptimal RFA effect was high in the tumors sized 2.0 cm or larger. Even in the tumors of >1.0 cm but ≤2.0 cm in size microscopically, 27% of cases did not show a 100% of RFA effect. From the present data, tumor size of ≤1.5 cm, strictly ≤1.0 cm, could be an indication for RFA if a complete histological therapeutic effect is mandatory.

There are still challenges in determining the therapeutic effects of RFA. Judgments of the RFA therapeutic effects between HE and NADH-diaphorase staining, even by examining serial tissue sections, do not always agree. In the Chiba Cancer Center, RFA therapy and subsequent follow-up revealed cases in which HE findings showed effectiveness, but the results of NADH-diaphorase staining were positive, or cases in which HE showed no changes but the results of NADH-diaphorase staining were negative (Yamamoto N., personal communication). Data acquisition from a larger number of cases and establishment of uniform criteria for evaluation of histopathology determining therapeutic RFA effects, including researching on how the NADH-diaphorase findings should be incorporated into such criteria, are important next stages of research.

From Table 1, the diameter of the area with a RFA effect usually exceeds the tumor size by several times, including the intraductal component. The effect of RFA appeared to extend in a radial direction. We need to be concerned about the effects of this technique on the superficial and deep sides of the mammary gland. Histologically, 1 of 28 patients suffered ulceration by the heat injury on the overlying skin (no. 3 in Table 1). Pectoral

muscle was not resected in any of the patients, but in 11 of the 28 patients, the deepest area of the resected specimen widely showed a RFA effect (e.g., Fig. 4). In these patients, it is unclear if thr pectoral muscle suffered significant injury from RFA, and close follow-up is necessary.

Acknowledgments This work was supported in part by a grant-in-aid for scientific research from the Ministry of Health, Labor, and Welfare.

Conflict of interest The authors and their immediate family members have no conflicts of interest.

References

1. Shimosato Y. Histopathological studies on irradiated lung tumors. Gann. 1964;55:521–35.
2. Japanese Research Society for Gastric Cancer. The general rules for the gastric cancer study. The 11th edition. Tokyo: Kanehara Shuppan; 1985. pp. 126–35.
3. Fisher B, Brown A, Mamounas E, Wieand S, Robidoux A, Margolese RG, et al. Effect of preoperative chemotherapy on local-regional disease in women with operable breast cancer: findings from National Surgical Adjuvant Breast and Bowel Project B-18. J Clin Oncol. 1997;15:2483–93.
4. Kuroi K, Toi M, Tsuda H, Kurosumi M, Akiyama F. Issues in the assessment of pathologic effect of primary systemic therapy for breast cancer. Breast Cancer. 2006;13:38–48.
5. Kuroi K, Toi M, Tsuda H, Kurosumi M, Akiyama F. Unargued issues on the pathological assessment of response in primary systemic therapy for breast cancer. Biomed Pharmacother. 2005; 59(Suppl 2):S387–92.
6. Buzdar AU, Ibrahim NK, Francis D, Booser DJ, Thomas ES, Theriault RL, et al. Significantly higher pathologic complete remission rate after neoadjuvant therapy with trastuzumab, paclitaxel, and epirubicin chemotherapy: results of a randomized trial in human epidermal growth factor receptor 2-positive operable breast cancer. J Clin Oncol. 2005;23:3676–85.
7. Mukai H, Watanabe T, Mitsumori M, Tsuda H, Nakamura S, Masuda N, et al. Final analysis of a safety and efficacy trial of preoperative sequential chemo-radiation therapy for the nonsurgical treatment (NST) in early breast cancer (EBC): Japan Clinical Oncology Group trial (JCOG0306). J Clin Oncol. 2010;28:7s (abstract).
8. Toi M, Nakamura S, Kuroi K, Iwata H, Ohno S, Masuda N, et al. Phase II study of preoperative sequential FEC and docetaxel predicts of pathological response and disease free survival. Breast Cancer Res Treat. 2008;110:531–9.
9. Kinoshita T, Iwamoto E, Tsuda H, Seki K. Radiofrequency ablation as local therapy for early breast carcinomas. Breast Cancer. 2010. doi:10.1007/s12282-009-0186-9.
10. Yamamoto N, Fujimoto H, Nakamura R, Arai M, Yoshii A, Kaji S, et al. Pilot study of radiofrequency ablation therapy without surgical excision for T1 breast cancer: evaluation with MRI and vacuum-assisted core needle biopsy and safety management. Breast Cancer. 2010. doi:10.1007/s12282-010-0197-6.
11. Seki K, Tsuda H, Iwamoto E, Kinoshita T. Histopathological effect of radiofrequency ablation therapy for primary breast cancer, with special reference to changes in cancer cells and stromal structure and a comparison with enzyme histochemistry. Breast Cancer. 2010. doi:10.1007/s12282-010-0215-8.
12. Imoto S, Wada N, Sakemura N, Hasebe T, Murata Y. Feasibility study on radiofrequency ablation followed by partial mastectomy for stage I breast cancer patients. Breast. 2009;18:130–4.

Breast Cancer (2011) 18:299–308
DOI 10.1007/s12282-010-0212-y

ORIGINAL ARTICLE

Early metabolic response to neoadjuvant letrozole, measured by FDG PET/CT, is correlated with a decrease in the Ki67 labeling index in patients with hormone receptor-positive primary breast cancer: a pilot study

Shigeto Ueda · Hitoshi Tsuda · Toshiaki Saeki · Jiro Omata · Akihiko Osaki · Takashi Shigekawa · Jiro Ishida · Katsumi Tamura · Yoshiyuki Abe · Tomoyuki Moriya · Junji Yamamoto

Received: 22 February 2010 / Accepted: 19 May 2010 / Published online: 9 July 2010

Abstract
Purpose To assess whether the early metabolic response evaluated by ^{18}F-fluorodeoxy-glucose positron emission combined with computed tomography (FDG PET/CT) predicts the morphological, pathological, and cell-cycle responses to neoadjuvant endocrine therapy of hormone receptor-positive primary breast cancer.
Study design Eleven patients (12 tumors) with estrogen receptor-positive (Allred score 7 or 8) primary breast cancer were enrolled. All patients received a daily dose (2.5 mg) of letrozole for 12 weeks followed by surgery. Sequential FDG PET/CT scans were performed before treatment (baseline), at 4 weeks after the initiation of endocrine therapy (PET2), and prior to surgery (PET3). Tumors showing a 40% or more reduction and those showing a less than 40% reduction in the standardized uptake value maximum (SUV_{max}) at PET2 compared with the baseline PET were defined as metabolic responders and metabolic nonresponders, respectively. Change in tumor size as measured by ultrasound (morphological response), pathological response, and change in the Ki67 labeling index in tumor tissue (cell-cycle response) during the neoadjuvant letrozole therapy were compared between the metabolic responders and nonresponders.

S. Ueda · J. Omata · T. Moriya · J. Yamamoto
Department of Surgery, National Defense Medical College, 3-2 Namiki, Tokorozawa, Saitama 359-8513, Japan
e-mail: syueda2000@yahoo.co.jp

J. Omata
e-mail: dr20008@ndmc.ac.jp

T. Moriya
e-mail: tmoriya@ndmc.ac.jp

J. Yamamoto
e-mail: jyamamot@ndmc.ac.jp

T. Saeki · A. Osaki · T. Shigekawa
Breast Oncology Service, Tokorozawa Ichou Hospital, 1-7-25 Nishi-tokorozawa, Tokorozawa, Saitama, Japan
e-mail: tsaeki@saitama-med.ac.jp

A. Osaki
e-mail: aosaki@saitama-med.ac.jp

T. Shigekawa
e-mail: takshige@saitama-med.ac.jp

S. Ueda · T. Saeki · T. Shigekawa
Department of Breast Oncology, Saitama Medical University, International Medical Center, 1397-1 Yamane, Hidaka, Saitama 350-1298, Japan

A. Osaki
Department of Breast Oncology, Saitama Medical University, 38 Morohongo, Moroyama, Saitama 350-0495, Japan

J. Ishida · K. Tamura · Y. Abe
Tokorozawa PET Diagnostic Imaging Clinic, 7-5 Higashi-Sumiyoshi, Tokorozawa, Saitama 359-1124, Japan
e-mail: ishida@toko-pet.or.jp

K. Tamura
e-mail: tamurak@nn.iij4u.or.jp

Y. Abe
e-mail: abe@toko-pet.co.jp

H. Tsuda (✉)
Department of Basic Pathology, National Defense Medical College, 3-2 Namiki, Tokorozawa, Saitama 359-8513, Japan
e-mail: hstsuda@ncc.go.jp

S. Ueda
Headquarter Clinic, Mutual Aid Association, Ministry of Defense, 5-1 Honmura-chou, Ichigaya, Shinjuku-ku, Tokyo, Japan

Results The average decreases in SUV_{max} at PET2 compared with the baseline PET in the metabolic responders ($n = 6$) and the metabolic nonresponders ($n = 6$) were 60.9% (±21.3 SD) and 14.2% (±12.0 SD), respectively. At PET3 compared with the baseline PET, the metabolic responders showed a significantly higher decrease of 64.5% (±18.7 SD) ($p = 0.0004$), whereas the nonresponders showed a nonsignificant decrease of 16.7% (±14.1 SD) ($p = 0.06$). The morphological and pathological responses after letrozole therapy did not differ between the metabolic responders and nonresponders. The metabolic responders showed a marked decrease in the Ki67 labeling index at 2 weeks after the initiation of treatment (62.9%, ±35.9 SD, $p = 0.04$) and at surgery (91.7%, ±10.7 SD, $p = 0.03$) compared with the baseline values. In contrast, metabolic nonresponders showed no significant change in the Ki67 index either after 2 weeks of therapy or at surgery.

Conclusion Cell-cycle response monitored by the Ki67 labeling index correlates with metabolic response monitored by tumor SUV_{max}. Monitoring of tumor SUV_{max} using FDG PET/CT may be feasible to predict cell-cycle response to neoadjuvant endocrine therapy of primary breast cancer.

Keywords Breast cancer · FDG PET/CT · Neoadjuvant endocrine therapy · SUV

Introduction

Neoadjuvant endocrine therapy is a treatment option for patients with hormone receptor (HR)-positive (estrogen receptor-positive and/or progesterone receptor-positive) breast cancer, and the long-term efficacy of this approach is currently being studied [1, 2]. Some clinical trials have shown that neoadjuvant endocrine therapy can contribute to down-staging and to improved therapeutic efficacy in HR-positive breast cancers [3–5]. Therefore, early identification of patients who do or do not respond to endocrine therapy is essential, allowing patients with less endocrine-sensitive tumors to receive alternative treatments such as surgery or chemotherapy [6].

A randomized trial (Intermediate Marker Project: Anastrozole, Combination or Tamoxifen; IMPACT) compared the efficacy of neoadjuvant anastrozole versus neoadjuvant tamoxifen for 12 weeks in 330 postmenopausal women with HR-positive operable breast cancer [4]. The rate of breast-conserving surgery was significantly higher in the anastrozole group (45.7%) than in the tamoxifen group (22.2%) ($p = 0.03$). In an affiliated study of the IMPACT trial, the Ki67 labeling index as a proliferation biomarker was measured at the 2nd week and at the 12th week of endocrine therapy prior to surgery. The mean Ki67 labeling indices at the 2nd week and the 12th week were decreased further in the anastrozole group than in the tamoxifen group ($p = 0.004$) [7]. Furthermore, the decreases in Ki67 labeling indices after 2 and 12 weeks of endocrine therapy were significantly correlated with relapse-free survival of the patients after surgery [8]. These results suggest that early cell-cycle response to endocrine therapies as measured by the Ki67 labeling index is predictive of better clinical outcome in patients with HR-positive breast cancer [9]. In the P024 trial of neoadjuvant letrozole for 337 women with HR-positive breast cancer, the objective response rate on clinical palpation was significantly higher in the letrozole group (55%) than in the tamoxifen group (36%) after the treatment for 12 weeks prior to surgery ($p < 0.001$) [10].

Currently, ^{18}F-fluorodeoxyglucose (FDG) positron emission tomography (PET) for imaging is widely used as a non-invasive approach for the detection and staging of breast cancer [11]. FDG PET provides the standardized uptake value (SUV) of tumor glucose metabolism as a highly reproducible quantitative parameter [12, 13]. The response of tumors to chemotherapy can be quantified by measuring changes in tumor glucose metabolism using sequential FDG PET [14, 15]. Small-scale clinical trials have revealed that an early metabolic response of the tumor after one or two cycles of chemotherapy correlates with better clinical outcome of the patients [16–18].

By means of cDNA microarray and immunohistochemistry, we previously reported that expression levels of cell-cycle-related proteins (Ki67 and CENP-F) were increased in tumors showing high FDG uptake in comparison with tumors showing low FDG uptake, suggesting that the level of FDG uptake could be explained, at least in part by the early stage proliferative activity of breast cancer cells [19].

The aim of the present study was to evaluate the feasibility of FDG PET in combination with computed tomography (FDG PET/CT) monitoring as a modality to predict the effect of endocrine therapy in primary breast cancers. This pilot study of neoadjuvant setting was designed to assess the utility of FDG PET/CT for the prediction of response of node-negative and HR-positive breast cancers to letrozole in postmenopausal women, taking into account morphological and pathological responses, and the cell-cycle response measured by the Ki67 labeling index in the primary tumors.

Materials and methods

Patients

Eleven patients with HR-positive operable (T1-T2, N0, M0) breast cancer were prospectively recruited for this

study between December 2007 and March 2008. One patient had bilateral tumors, and thus a total of 12 tumors were assessed. To determine baseline staging of breast cancer, palpation, chest X-ray, ultrasound of the bilateral breast, axilla, and liver, as well as whole-body FDG PET/CT were performed. In all the 11 patients, no axillary involvement was detected by palpation, ultrasound, or FDG PET/CT.

Estrogen receptor (ER), progesterone receptor (PR), and c-erbB2 (HER2) were assessed immunohistochemically in specimens obtained by core needle biopsy. Inclusion criteria for this study were postmenopausal women having breast cancer with ER positivity (Allred score 4 or more) and/or PR positivity (Allred score 4 or more) and in whom chemotherapy was not indicated or who refused chemotherapy. Exclusion criteria were metastatic disease and severe diabetes mellitus.

Patients received a daily dose of letrozole (2.5 mg) for at least 12 weeks before surgery (Fig. 1). Core needle biopsy (CNB) was performed for all patients at baseline and at 2 weeks after initiation of endocrine therapy.

FDG PET/CT scans were performed before initiation of endocrine therapy (baseline PET), at 4 weeks after initiation of therapy (PET2), and prior to surgery (PET3). We considered FDG PET/CT scanning at 4 weeks after initiation of treatment was the best timing of early response assessment of SUV for the purpose of minimizing the effect of tissue repairing reaction to CNB. All patients underwent breast-conserving surgery or mastectomy at the Departments of Surgery of the National Defense Medical College (NDMC) Hospital or the Tokorozawa Icho Hospital, Tokorozawa, Japan.

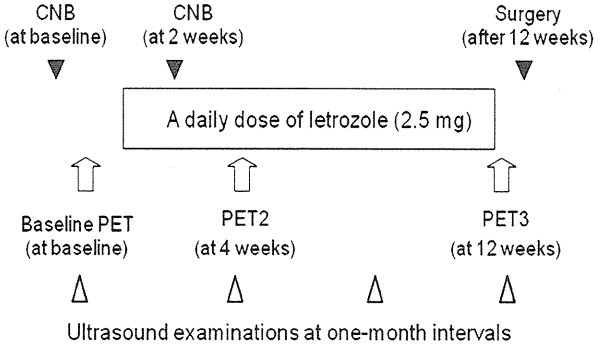

Fig. 1 Schematic presentation of the study design. The regimen of neoadjuvant endocrine therapy consisted of a daily dose (2.5 mg) of letrozole for 12 weeks. The treatment was monitored by serial FDG PET/CT at baseline (*baseline PET*), at 4 weeks (*PET2*) after the initiation of endocrine therapy, and at 12 weeks (*PET3*) after the initiation of endocrine therapy and prior to surgery. Ultrasound examination to measure tumor size was also performed at baseline and on a monthly basis. Evaluation of tumor size using ultrasound according to the RECIST guidelines [16] was performed by one experienced ultrasonographer to compare size reduction between baseline and the time at the completion of treatment. The intercurrent measurements of tumor size by ultrasound were for determination of progression; hence, discontinuation of the treatment was considered. Core needle biopsies for tumors were performed at baseline and at 2 weeks after the initiation of treatment. Surgery was performed after the completion of the endocrine therapy. The Ki67 labeling index of cancer cells was evaluated both in core needle biopsy specimens and in surgically resected specimens

This study was approved by the institutional review committee of the NDMC. Informed consent was obtained from each eligible patient.

FDG PET/CT and quantification of FDG uptake in primary tumors

The procedure for FDG PET/CT has been described previously [13]. Briefly, patients underwent ^{18}F-FDG PET/CT scans at Tokorozawa PET Imaging and Diagnostic Clinic (Tokorozawa, Japan). PET/CT imaging was performed with Biograph Duo (Siemens CTI). The Biograph Duo allows simultaneous collection of 64 slices over a span of 15.8 cm with a slice thickness of 2.5 mm and a transaxial resolution of 6.3 mm. All data were reconstructed with OSEM image. Patients fasted at least 6 h before PET/CT studies. One hour after intravenous administration of ^{18}F-FDG at about 3.7 MBq/kg, a transmission scan using CT for attenuation correction and anatomical imaging was acquired for 90 s. Blood glucose levels measured in each patient did not exceed 120 mg/dl.

A region of interest (ROI) was placed in the target lesions, including the highest uptake area (circle ROI, 10 mm in diameter), and SUV_{max} in the ROI was calculated. SUV_{max} is decay-corrected tissue activity divided by the injected dose per patient body. SUV_{max} was calculated using the following formula: SUV = activity in ROI (MBq/ml)/injected dose (MBq/kg body weight).

After the completion of FDG PET acquisition, the reconstructed attenuation corrected PET images, CT images, and combined images of matching pairs of the FDG PET and CT images were available for review in axial, coronal, and sagittal planes and in maximum intensity projections, three-dimensional cine-mode. At least two experienced nuclear medicine radiologists interpreted the FDG PET/CT images.

Criteria for morphological response on ultrasound imaging

Patients underwent ultrasound examination to measure tumor size during treatment. Evaluation of tumor size using ultrasound was performed twice by one experienced ultrasonographer to compare size reduction: at baseline and at the completion of treatment, according to the RECIST guidelines [16]. The longest diameter of a target lesion was

determined as the clinical tumor size. Intercurrent measurements of tumor size by ultrasound were performed only for the detection of patients with progressive disease.

The protocol stipulated that use of letrozole should be discontinued in patients who showed progressive disease (20% or more increase in size) by ultrasound and that such patients should be excluded from further participation in the study. However, no patients in this series had progressive disease.

Criteria for pathological response

Histological criteria for assessment of therapeutic response in breast cancer were taken from the General Rules for Clinical and Pathological Recording of Breast Cancer 2007 [20]. Pathological response was evaluated only from histological changes in the invasive area, and the presence of ductal components and/or lymph node metastasis was not evaluated. Pathologic complete response or pCR (Grade 3) was defined as the complete disappearance of invasive components of breast cancer in the pathologic specimen. The disappearance or marked degeneration of two-thirds or more of the tumor cells was defined as substantially effective (grade 2). The disappearance or marked degeneration of one-third to less than two-thirds was defined as moderately effective (grade 1b). The disappearance or marked degeneration of less than one-third of the tumor cells or mild tumor cell degeneration, regardless of the percentage, was defined as mildly effective (grade 1a). Almost no change in cancer cells after treatment was defined as not effective (grade 0). Pathological response was based on microscopic assessment of the surgical specimen by one breast pathologist (H.T.).

Pretherapeutic clinical and immunohistochemical parameters

Before the initiation of endocrine therapy, CNB was performed for diagnosis. Patient age, tumor size, histology, and the absence of clinically positive lymph nodes were recorded. Expressions of estrogen receptor (ER), progesterone receptor (PR), and c-erbB2 (HER2) were measured as described previously [21–23]. Scores for ER and PR were measured by the Allred scoring system [24].

Scoring of the Ki67 labeling index

Immunohistochemically, the Ki67 labeling index was measured to evaluate the proliferative activity of cancer cells. The Ki67 labeling index was counted for a minimum total of 300 cancer cells from 10 randomly selected high-power fields (400×) containing representative sections of the tumors. The value was calculated as the percentage of cells showing moderate to high staining intensity relative to the total number of cells [8, 9].

Statistical analysis

Statistical analysis was carried out with Statview 5.0 (SAS Institution Inc., Cary, NC). The Mann-Whitney U test and Student's t test were used to compare variables between metabolic responders and nonresponders. The Wilcoxon signed-ranks test was used to compare serial changes in Ki67 values between metabolic responders and metabolic non-responders. A simple regression analysis was used to determine the relationship between percentage reduction in SUV_{max} and percentage decrease in the Ki67 labeling index by a head-to-head comparison of each case. Differences at a p value of less than 5% were considered to be statistically significant.

Results

Patient characteristics

Table 1 shows the characteristics of 12 clinically node-negative tumors in 11 patients. The average patient age was 73.6 years [±9.3 standard deviation (SD)]. Eleven (92%) of the 12 tumors were invasive ductal carcinoma, and one (8%) was mucinous carcinoma. Average tumor size was 26.5 mm (±9.5 SD). Ten (83%) and 2 (17%) of the 12 tumors were ER-positive with Allred scores of 8 and 7, respectively. For PR status, four (33%) and two (17%) tumors had Allred scores of 8 and 7, respectively. In three (25%) tumors, the Allred score was 5 or 4, and in three tumors (25%) the Allred score was 0 or 1. Two (17%) of the 12 tumors exhibited HER2 overexpression (score 3+). There was no correlation of baseline SUV_{max} with PR or HER2 status.

Metabolic response by FDG PET/CT

Baseline PET and PET2 were performed for all 12 tumors. PET2 was performed on average 31.8 ± 4.3 days after initiation of endocrine therapy. PET3 was performed for 10 (83%) of the 12 tumors at 106.5 ± 16.3 days after initiation of treatment. The other two (17%) patients refused to undergo FDG PET/CT scanning at PET3 (Table 2).

Changes in SUV_{max} were compared among baseline PET, PET2, and PET3 (Fig. 2a). These results demonstrated the existence of a clear threshold at the point of PET2 between tumor no. 5 (31.4% reduction) and tumor no. 2 (43.4% reduction). We adopted 40% reduction in SUV_{max} as a tentative cutoff value between metabolic responders and metabolic nonresponders.

Table 1 Characteristics of the 12 clinically node-negative primary breast cancers in 11 patients

Serial number	Location	Age (year)	Tumor size (mm)	Histology	Allred score		HER2
					ER	PR	
1	Rt	80	36	Invasive ductal	7	0	3+
2	Lt	81	27	Mucinous	8	4	2+
3	Rt	78	33	Invasive ductal	8	1	3+
4	Lt	60	25	Invasive ductal	8	8	1+
5	Rt	77	27	Invasive ductal	8	5	1+
6	Lt	77	19	Invasive ductal	8	8	1+
7	Lt	82	49	Invasive ductal	7	7	2+
8	Rt	83	12	Invasive ductal	8	5	1+
9	Rt	70	23	Invasive ductal	8	8	2+
10	Lt	68	20	Invasive ductal	8	7	1+
11	Lt	70	22	Invasive ductal	8	0	0
12	Lt	75	24	Invasive ductal	8	8	0

Numbers 5 and 6 are bilateral tumors from a single patient

ER estrogen receptor, *PR* progesterone receptor, *Lt* left, *Rt* right

Table 2 SUV_{max} of tumors assessed by FDG PET/CT at baseline and at 4 and 12 weeks after initiation of neoadjuvant letrozole therapy, stratified by metabolic responders and metabolic nonresponders

Serial number	SUV_{max} by FDG PET/CT		
	Baseline	At 4 weeks	At 12 weeks
Responders			
2	3.48	1.97	1.64
6	6.01	3.13	2.44
8	1.88	0.91	ND
9	12.7	3.82	3.23
10	5.18	2.66	1.32
11	12.8	5.66	5.82
Average (±SD)	6.8 (4.8)	2.8 (1.9)	2.9 (2.0)
Nonresponders			
1	4.92	5.29	4.91
3	2.36	2.17	2.28
4	3.11	2.38	2.3
5	3.22	2.21	2.41
7	2	1.57	1.68
12	1.25	0.96	ND
Average (±SD)	2.8 (1.6)	2.4 (1.5)	2.7 (1.3)

ND not done, *SD* standard deviation

Metabolic responders and metabolic nonresponders comprised six (50%) tumors and six (50%) tumors, respectively. The average reduction in SUV_{max} at PET2 compared with the baseline PET was 60.9% (±21.3 SD) in metabolic responders ($p = 0.0009$) and 14.2% (±12.0 SD) in metabolic nonresponders ($p = 0.03$). In contrast, the average reduction in SUV_{max} at PET3 compared with the baseline PET was 64.5% (±18.7 SD) in metabolic responders ($p = 0.0004$) and 16.7% (±14.1 SD) in metabolic nonresponders ($p = 0.06$) (Fig. 2b). Figure 3 shows serial FDG PET/CT images of tumors in a metabolic responder (upper panels) and a metabolic nonresponder (lower panels).

Two patients having HER2-overexpressing tumors were included in the non-responding group. PR status was not correlated with metabolic response (data not shown).

Morphological response on ultrasound imaging

Tumors with a metabolic response showed an average 3.2-mm reduction in size, ranging from 0.5 to 5.9 mm ($p = 0.3$), whereas tumors with a metabolic nonresponse also showed an average 3.2-mm reduction in size, ranging from −4.4 to 10.4 mm ($p = 0.5$). There was no difference between the two groups (Fig. 4).

Pathological response

Pathologic response of the six metabolic responders fell into grade 1b in two (33%), grade 1a in three (50%), and grade 0 in one (17%). On the other hand, pathologic response of the six non-responders fell into grade 1a in four (67%) and grade 0 in two (33%). There were no tumors with an effect of grade 2 or 3. When tumors achieved grade 1b were classified as pathologic responder and tumors with grade 0 and grade 1a were classified as non-responders, two pathologic responders belonged to metabolic responders, although there was no statistical difference in pathologic response rate between metabolic responders and metabolic nonresponders ($p = 0.5$).